RSC Advances

Study of the temperature and solvent content effects on the structure of Cu-BTC metal organic framework for hydrogen storage

Journal:	*RSC Advances*
Manuscript ID:	RA-ART-01-2015-001890.R1
Article Type:	Paper
Date Submitted by the Author:	24-Feb-2015
Complete List of Authors:	Khoshhall, Saeed; Babol University of Technology, Chemical Engineering Ghoreyshi, Ali Asghar; Babol University of Technology, Chemical Engineering Department Jahanshahi, Mohsen Jahanshahi; Babol University of Technology, Mohammadi, Maedeh; Babol University of Technology, Chemical Engineering

RSC Advances

RSCPublishing

ARTICLE

Study of the temperature and solvent content effects on the structure of Cu-BTC metal organic framework for hydrogen storage

Saeed Khoshhal[a], Ali Asghar Ghoreyshi[a*], Mohsen Jahanshahi[a] and Maedeh Mohammadi[a]

Metal organic frameworks (MOFs) with intriguing structural motifs and unique properties are potential candidates for hydrogen storage. In this study, Cu-BTC (Copper (II) benzene-1,3,5-tricarboxylate) MOF was synthesized using ultrasonic followed by reflux method. The influence of synthesis temperature (80, 110 and 140 ^{o}C) and solvent content (50, 75 and 100 ml DMF) on the structure and H_2 storage performance of developed MOFs was investigated. The structure of synthesized MOFs was characterized by XRD, TGA/DSC, FE-SEM and BET analyses. Hydrogen adsorption performance of the developed MOFs was evaluated using volumetric technique. The highest H_2 uptake of 0.7 wt% was obtained with the sample synthesized at 80 ^{o}C with 75 ml DMF. The isosteric heat of adsorption was calculated by substitution of Freundlich equation with temperature dependent parameters in Clausius-Clapeyron equation. The isosteric heat of hydrogen adsorption monotonically decreased with surface loading. Also, the *n*-th order kinetic model was successfully applied to describe the experimental kinetic data in which the order of adsorption reaction was considered as an adjustable parameter. The value of 1.59 obtained for the order of kinetic model indicated that the adsorption process mechanism followed a combination of physisorption and chemisorption.

Introduction

Soil, air and water pollutions caused by human activities have had serious effects on all living creatures. One of the greatest dilemmas in environmental pollution issues is the effect of greenhouse gases on the Earth's climate. The famous one of these gases is carbon dioxide that greatly contributes to the global warming phenomenon. This gas is released into the atmosphere by combustion of fossil fuels in automobiles, residential sectors, factories and power generation plants. The main solution suggested by scientists to alleviate this issue is use of alternative energy rather than fossil fuels to reduce carbon emission into the atmosphere. Hydrogen as a carbon-neutral fuel is a good response to this necessity. However, there are some key challenges which need to be addressed before taking advantage of this alternative fuel including its production, purification, storage, transmission and conversion [1]. Physical adsorption is a promising route for effective hydrogen storage and separation. This technology offers not only operational simplicity but also greater energy efficiency. Hydrogen can be physically adsorbed by various types of adsorbents including graphene sheets [2], zeolites [3], carbon nanotubes [4, 5], and activated carbons [6, 7].

New classes of crystalline materials containing a metal in centre connected by organic ligands, which are called metal organic framework (MOF), were first used for hydrogen adsorption by Rosi

et al. [8]. MOFs are new categories of porous materials with large surface area and high pore volume. There are a great deal of researches that reveal the potential capability of MOFs for applications in Li-ion batteries [9], sensors [10, 11], drug delivery [12], catalysts [13, 14] and gas adsorption and separation [1, 15-20]. These materials seem to offer viable solution for H_2 capture and storage because of their high sorption capacity compared to other adsorbents[21]. Hydrogen storage performance of MOFs was tested at the pressure range of 1 to 100 bar to ensure safety in automotive applications [22]. Wong-Fog et al. synthesized a Zn-based MOF, named MOF-5, which displayed a hydrogen uptake of 5 wt% at 77 K and 90 bar [23]. Another Zn-based MOF, named MOF-177, prepared by Chae et al. showed a hydrogen capacity of 7.5 wt% at 77 K and 80 bar [24]. Li and Yang reported hydrogen uptake of 1.45 wt% at 77 K and 1 bar and 0.6 wt% at 298 K and 100 bar on MOF-177 [25]; however, Saha et al. achieved a hydrogen capacity of 1.36 wt% at 77 K and 1 bar and 0.35 wt% at 298 K and 40 bar [26]. Abid et al [27] synthesized a Zr-based MOF, named UiO-66, which exhibited a hydrogen uptake of 1.8 wt% at 77 K and 2 bar; this uptake capacity could be increased to 4.2 wt% by increasing pressure up to 60 bar; nevertheless, this adsorbent adsorbed 0.5 wt% of hydrogen at 296 K and 60 bar.

Several methods have been used for development of MOFs including hydro/solvothermal method [13, 19, 28], atmospheric pressure and reflux [20], microwave [29], ultrasonic [17, 30] and electrochemical and mechanochemical approaches [31]. However, in all implemented methods, MOFs with high purity can be obtained just under optimized reactants composition and operating conditions. Operating conditions such as reaction time, pressure, pH and temperature are very important to obtain high quality MOF crystals [20, 32-34]. The crystal structure prediction, design and control of topology of MOFs can be possible just through a detailed study on these factors.

Cu-BTC (Copper(II) benzene-1,3,5-tricarboxylate) is considered as one of the potential MOF candidates for hydrogen storage [35]. Lin et al. [1] synthesized Cu-BTC in a sealed system using solvothermal method at 110℃ and reported an uptake of 0.47 wt% for hydrogen at 303 K and 35 bar. In another investigation performed by Yan et al. [19], Cu-BTC was synthesized using same method, but the synthesis temperature was lowered to 75℃. They obtained a MOF with very large surface area and high pore volume and used it for CO_2/CH_4 and CO_2/N_2 separation. They also found that the porosity properties of synthesized MOF could be further enhanced by increasing solvent removal efficiency from the MOF structure. As confirmed by many researchers, synthesis temperature is one of the most influential factors on structure and properties of MOFs. It has been reported that the dimensionality and metal ion coordination number of framework increased and the coordinated solvent molecules decreased when the synthesis temperature was raised [36-39]. Wang et al. [20] investigated sorption properties of CO_2/CO and CO_2/CH_4 on Cu-BTC using various solvents and synthesis methods at different temperatures. They reported that the crystallinity of frameworks enhanced when synthesis temperature was decreased. Yet an opposite trend has been reported by Forster et al. [40] who synthesized Co(II)-succinates MOF at five different temperatures. Their results revealed that the density and dimensionality of MOFs improved by increasing the temperature. Since there is not a consensus among researchers in this regards, this study focuses on the influence of synthesis temperature and solvent content on the H_2 sorption performance of Cu-BTC.

During hydro/solvothermal synthesis of MOFs in a sealed system, raising the temperature will produce autogenous pressure; however, when reflux condition or ultrasonic waves are used for synthesis, pressure remains constant. Therefore, a precise investigation about the effect of temperature on the structure of MOF could be easily done in the latter method. The main objective of the present study was to investigate the influence of temperature and solvent content on the structure of Cu-BTC which was synthesized via ultrasonic followed by reflux method and finding the optimum condition. The second objective was to assess the hydrogen storage capability of synthesized MOF samples. Finally, adsorption isotherm, kinetics and thermodynamics were analyzed using suitable physical models.

1. Materials and methods

1.1. Chemicals

The used chemicals including 1,3,5-benzenetricarboxylic acid (H_3BTC) and copper(II) nitrate trihydrate, were obtained from Merck, Germany and N,N-dimethylformamide (DMF) and ethanol were purchased from Scharlau, Spain. All the materials were analytical grade and used without further purification.

1.2. Materials synthesis

In order to prepare Cu-BTC (Copper(II) benzene-1,3,5-tricarboxylate), 1.5 g copper (II) nitrate trihydrate and 1 g 1,3,5-benzenetricarboxylic acid (H_3BTC) were added to a 200 ml beaker containing dimethylformamide (DMF) as solvent (50, 75 and 100 ml) and the mixture was sonicated for 30 min. The solution was then

heated (80, 110 and 140 °C) in an oil bath at reflux condition at atmospheric pressure for 12 h. Different experimental conditions at which Cu-BTC samples were synthesized are listed in Table 1. The as prepared samples were denoted as Cu-BTC X/Y, where X represents the solvent content (ml) and Y shows the synthesis temperature (°C). After this stage, the product was washed twice with DMF and then a mixture of ethanol and deionized water (volume ratio of 1:1); during this process some precipitates were formed. In order to activate Cu-BTC, the solvent should be removed from its structure. Therefore, the mixture of ethanol, deionized water and the precipitates was placed on a magnetic stirrer and stirred for 12 h. Then, the blue precipitates were isolated by centrifugation and dried at 80 °C for 8 h. Finally, the developed adsorbent was calcined at 180 °C for 12 h before using in hydrogen adsorption experiments.

Table 1: Experimental conditions considered for synthesis of Cu-BTC MOFs

Sample	$Cu(NO_3)_2.3H_2O$ (g)	BTC (g)	DMF (ml)	Sonication time (min)	Reflux temperature (˚C)	Production yield (%)
Cu-BTC 50/110	1.5	1	50	30	110	80
Cu-BTC 75/110	1.5	1	75	30	110	91
Cu-BTC 100/110	1.5	1	100	30	110	89
Cu-BTC 75/140	1.5	1	75	30	140	91
Cu-BTC 75/80	1.5	1	75	30	80	92

The amount of hydrogen adsorbed by the synthesized MOF was determined using a dual-cell volumetric system as described in our previous works [4-6].

1.3. Characterization of the synthetized MOFs

XRD patterns for the adsorbents were recorded at 298 K by a XPERT-PRO X-ray diffractometer with Cu-Kα radiation (λ=1.5406Å). Nitrogen adsorption/desorption isotherms were measured at 77 K over the relative pressure range of 0.01 to 0.99 using Belsorp max analyzer. Specific surface area was calculated by BET method and micropore properties of samples were determined by t-plot. The surface morphology and roughness was studied by MIRA3 TESCAN field emission scanning electron microscopy (FE-SEM). Thermogravimetric analysis (TGA) was carried out in a METTLER TOLEDO TGA/DSC 1 to investigate the thermal stability of the samples, differential scanning calorimetry (DSC) was also performed to study the thermal behaviour of the synthesized samples.

2. Results and discussion

2.1. Characterization results

The MOF samples were synthesized at 80, 110 and 140 °C, below the boiling point of solvent (about 153 °C). The XRD patterns obtained for these three samples are shown in Fig.1 which are in good agreement with those reported for Cu-BTC in the literature [1, 17, 28], confirming that a pure Cu-BTC phase formed. All samples demonstrated sharp peaks at 6.8^o, 9.6^o, 11.8^o and 13.5^o which can be respectively assigned to (200), (220), (222) and (400) crystal planes of Cu-BTC.

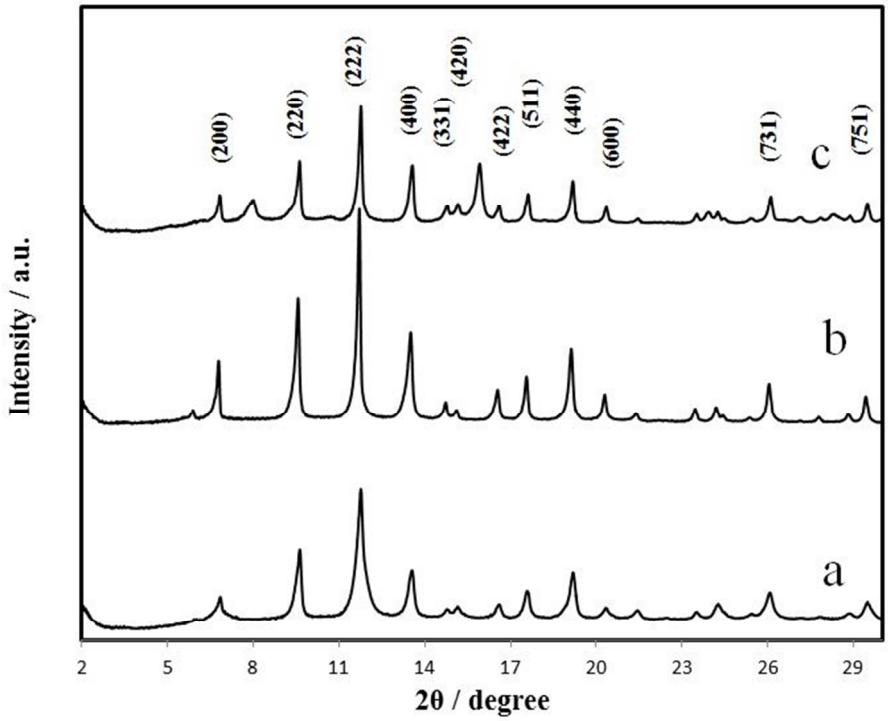

Fig.1. XRD patterns of Cu-BTC MOFs synthesized at (a) 80 °C, (b) 110 °C and (c) 140 °C

The relative crystallinity for each sample was determined by quantifying the area under the most predominant peaks (at $2\theta = 2^0$ to 30^0) using X'Pert Highscore plus software and then dividing this area to the area of the synthesized sample with highest crystallinity [41]. The relative crystallinity was 100, 95.97 and 61.25% for MOF samples synthesized at 80, 110 and 140 °C, respectively. This implies that the crystallinity of products increased by decreasing synthesis temperature. Synthesis at high temperature can produce some impurities such as Cu_2O during the formation of Cu-BTC framework. However, there are two new peaks located at $2\theta \sim 7.99^o$ and 15.92^o in the XRD pattern of sample prepared at 140 °C which implies that a different phase has been formed.

The textural properties of the synthesized Cu-BTC samples were analysed by N_2 adsorption/desorption at 77 K; the results are exhibited in Fig. 2. These flat-plateau isotherms are considered type I, as classified by IUPAC. This type of isotherm is characteristic of microporous materials. The textural properties of the synthesized MOFs are summarized in Table 2. The results show that the BET surface area, total pore volume and micropore volume increased by decreasing the synthesis temperature. The main reason for such enhancement is increasing the crystallinity at low temperature. Use of high synthesis temperature could conclude to the excess widening of micropores and creation of mesopores as evidenced by the broad hysteresis loop observed in the adsorption/desorption isotherm of MOF sample synthesized at 140 °C (Fig. 2).

RSC Advances RSCPublishing

ARTICLE

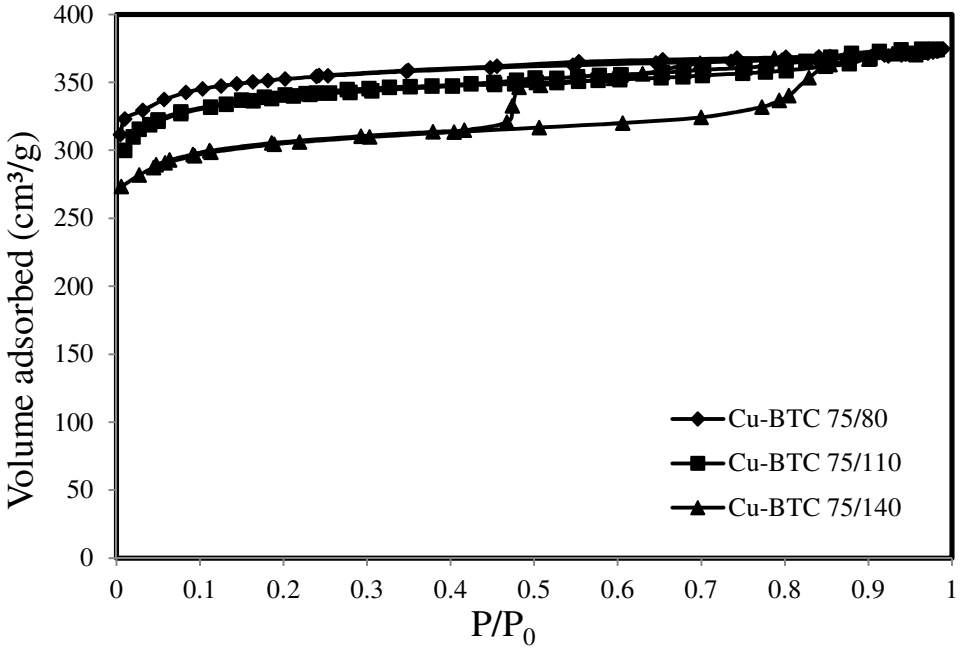

Fig.2. N_2 adsorption/desorption isotherms for Cu-BTC MOFs at 77 K

Table 2: The textural properties of the synthesized Cu-BTC MOFs

Sample	BET(m^2/g)	Pore vol. (cm^3/g) at P/P_0=0.50	Micro pore volume (cm^3/g)	Mean pore diameter (nm)
Cu-BTC 75/80	1386.9	0.560	0.475	1.67
Cu-BTC 75/110	1343.7	0.541	0.445	1.72
Cu-BTC 75/140	1210.5	0.490	0.426	1.91

The morphology, microstructure and particle shape of Cu-BTC MOFs were investigated by FE-SEM analysis; the SEM micrographs are depicted in Fig. 3. The developed MOF samples possess nearly identical particle size with octahedral morphology. The SEM micrographs also well demonstrate porous and rough surface of developed MOFs that it is favourable for hydrogen adsorption.

RSC Advances RSCPublishing

ARTICLE

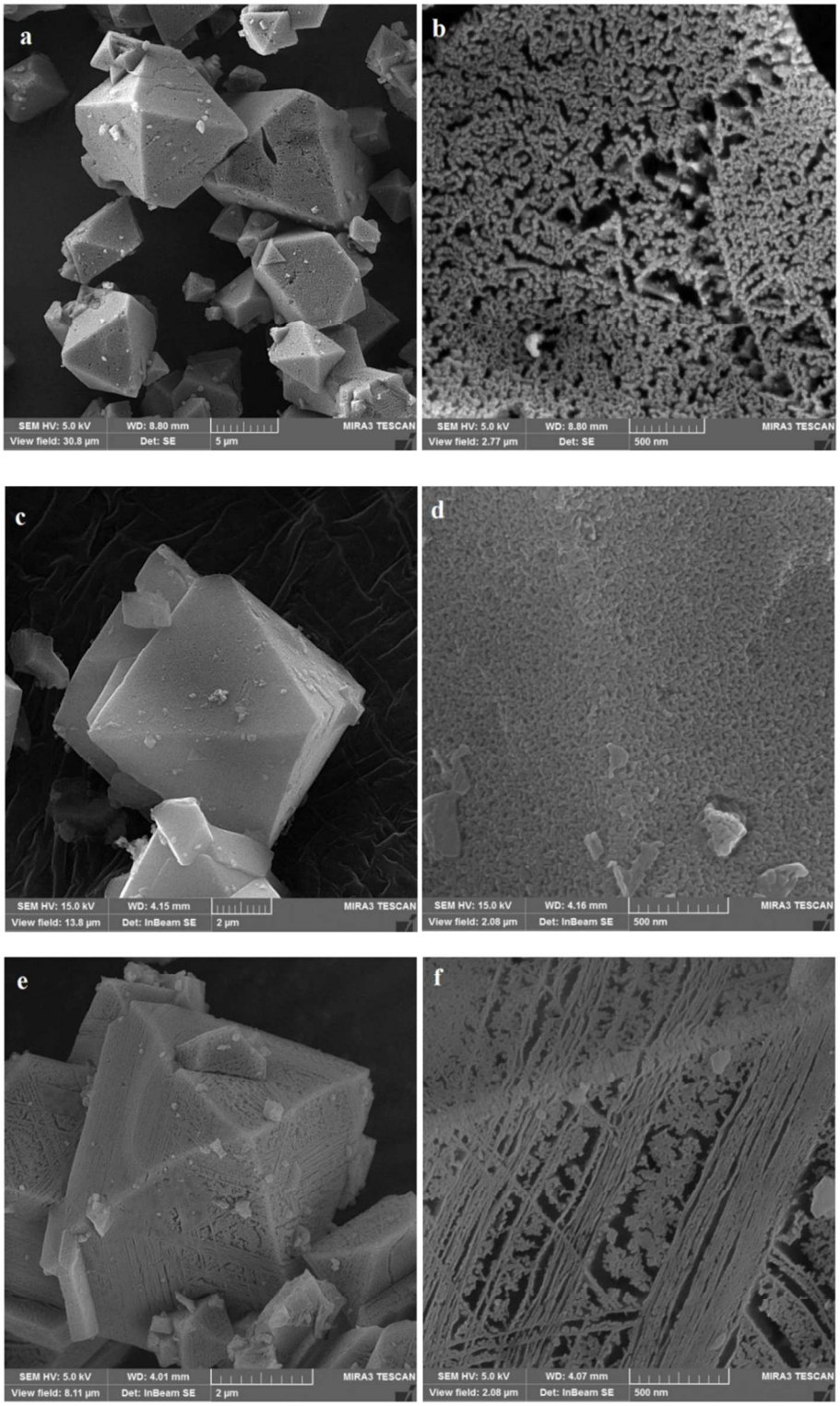

Fig.3. FE-SEM micrographs of Cu-BTC MOFs synthesized at (a and b) 80 °C, (c and d) 110 °C and (e and f) 140 °C

Figs. 4 a and b illustrate TGA/DSC analysis curves related to samples prepared at 80, 110 and 140 °C, respectively. In TGA curves of MOFs prepared at 80 and 110°C, there are two weight losses which respectively correspond to evaporation of moisture and solvent (first weight loss) and decomposition of MOF to copper oxide (second weight loss). Both processes are endothermic as confirmed by DSC analysis. However, in DSC curve of MOF synthesized at 140°C, an exothermic peak is observed. It is most probable that this sample, which had the lowest crystallinity, undergone a combustion process after decomposition of its constituents.

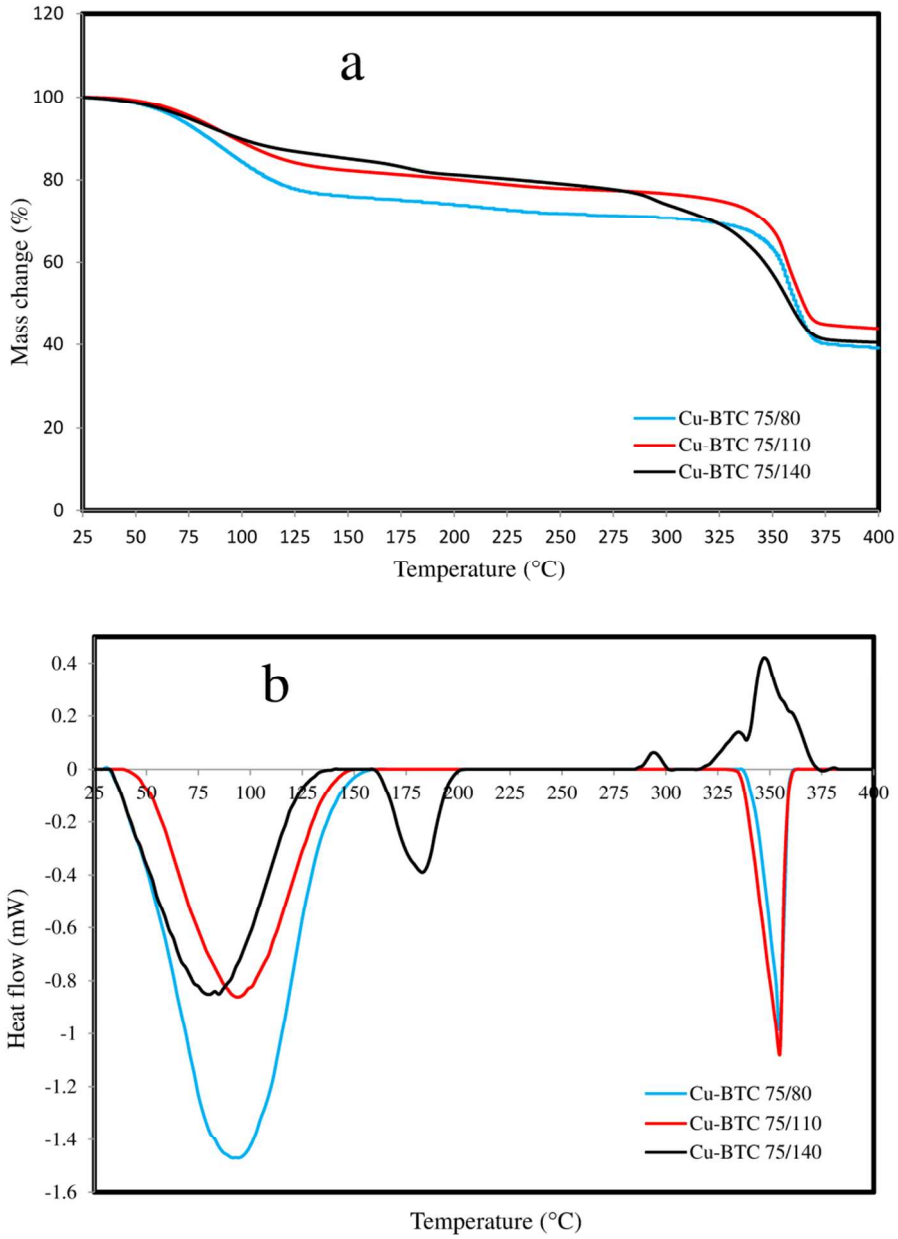

Fig.4. TGA (a) and DSC (b) curves of Cu-BTC MOFs synthesized at 80 °C, 110 °C and 140 °C

Table 3 summarizes the results of present study and those available in the literature for the synthesis of Cu-BTC MOFs. According to Table 3, the BET surface area of the Cu-BTC MOF synthesized in this work (1387 m^2/g) was comparable to

those prepared by solvothermal method wherein higher synthesis temperature and/or reaction time were implemented.

Table 3: Summary of the results of present work and literature for Cu-BTC MOF

Synthetic method	Reaction temperature/ power	Solvent	Reaction time	S_{BET} (m^2/g)	References
Ultrasonic	40 kHz /60 W	DMF, H_2O and EtOH	60 min	1100	[17]
Mechanochemical	-	H_2O, EtOH	10 min	739	[31]
Solvothermal	180℃	H_2O, EtOH	12 h	692	[28]
Solvothermal	120℃	H_2O, EtOH	12 h	-	[13]
Solvothermal	110℃	H_2O, EtOH	18 h	1055	[1]
Solvothermal	75 ℃	DMF	24 h	1922	[19]
Ultrasonic and reflux	80 ℃	DMF	12 h	1387	Present work

2.2. Hydrogen adsorption

2.2.1. Adsorption equilibria

2.2.1.1 Effect of solvent content and synthesis temperature

The H_2 adsorption experiments were first carried out for samples 1-3 to find optimum solvent amount at constant reaction temperature (110 °C) in order to maximize hydrogen adsorption. Experimental hydrogen adsorption data obtained at different solvent contents are exhibited in Fig. 5. As observed in this figure, at all implemented pressures, the hydrogen uptake increased as the quantity of DMF increased from 50 to 75 ml. The H_2 uptake was 0.27 and 0.65 wt% at 45 bar and 298 K for samples synthesized with 50 and 75 ml DMF, respectively. However, further increase of the solvent content from 75 to 100 ml did not enhance the H_2 uptake. Therefore, among the samples developed with different DMF contents, sample 2 which was prepared with 75 ml of solvent was chosen for further investigations.

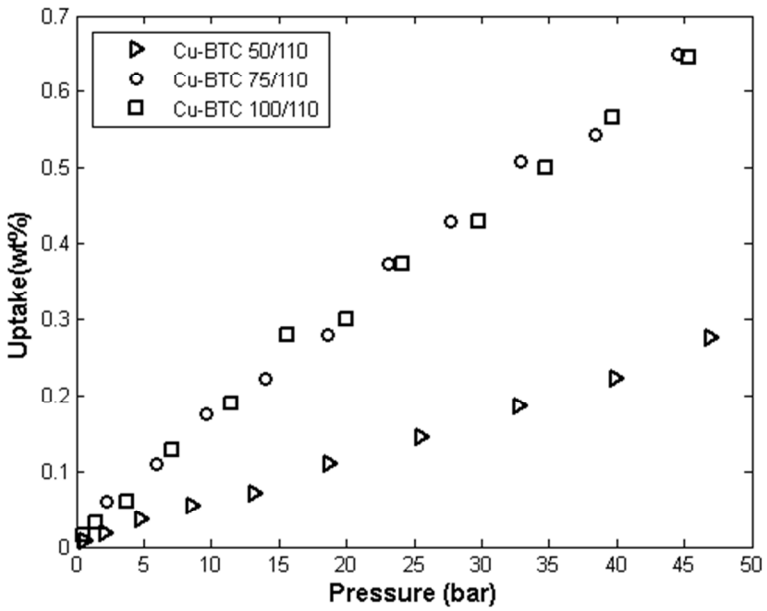

Fig.5. Experimental hydrogen adsorption data on Cu-BTC MOFs synthesized at 110℃ with different solvent contents

For the sake of examining the influence of synthesis temperature on the H_2 sorption performance of Cu-BTC adsorbent, several samples were synthesized at different temperatures, i.e. 80, 110 and 140℃. Fig. 6 displays experimental hydrogen uptake data versus pressure. The H_2 uptake at 45 bar and 298 K was 0.696, 0.650 and 0.586 for samples synthesized 80, 110 and 140℃, respectively. Results show that the uptake of H_2 at 45 bar for the MOF prepared at 80 °C was about 16% more than the one manufactured at 140 °C. Such results could be expected, as porosity and surface analysis showed the decrease of surface area and microporosity along with increase of synthesis temperature (Table 2). As a result, the sample prepared at highest temperature revealed the lowest hydrogen uptake. The H_2 uptake performance of the Cu-BTC sample synthesized in this work was compared to other MOFs reported in the literature as summarized in Table 4. As could be inferred from this comparison, the H_2 uptake of the developed MOF (Cu-BTC 75/80), obtained under optimized condition, at ambient temperature and high pressure was higher than those available in the literature. Such enhanced performance was confidently attributed to the influence of synthesis conditions including solvent content and synthesis temperature on the structural properties and thus uptake capacity of the MOF.

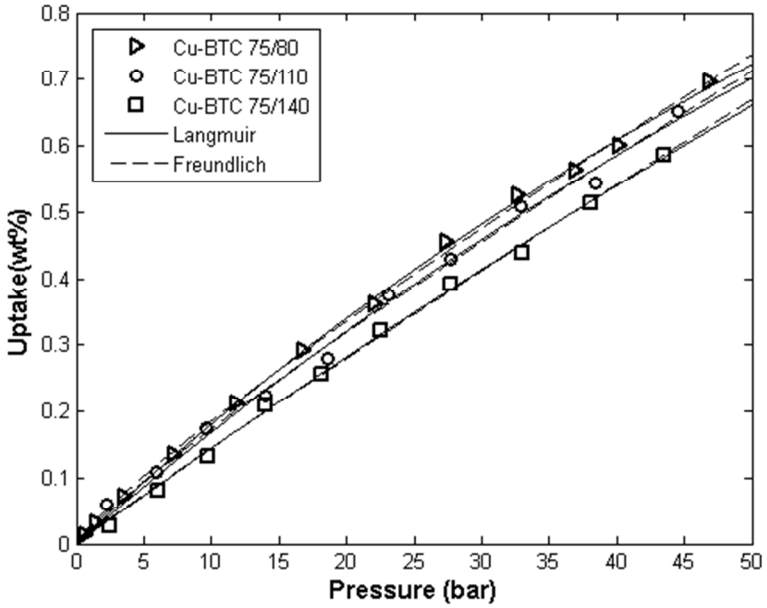

Fig.6. Experimental hydrogen adsorption data and the fitted curves by Langmuir and Freundlich isotherms for MOFs synthesized at 80, 110 and 140 °C at 298 K

Table 4: Summery of hydrogen uptake and BET surface area for several types of MOFs

MOF samples	BET surface area (m^2/g)	Hydrogen uptake at 77 K and 1 bar (wt%)	Hydrogen uptake at 77 K and high pressure (wt%)	Hydrogen uptake at ambient temperature and high pressure (wt%)	Ref.
MOF-177	3275	1.36	19.67 at 120 bar	0.35 at 298 K and 40 bar	[26]
MOF-177	3100	1.45	-	0.60 at 298 K and 100 bar	[25]
UiO-66	1434	1.8 at 2 bar	4.2 at 60 bar	0.50 at 296 K and 60 bar	[27]
MOF-200	4530	-	14 at 80 bar	-	[21]
MOF-210	6240	-	15 at 80 bar	-	[21]
MOF-74	950	1.34	1.97 at 88 bar		[23]
Cu-BTC	1944	1.60	3.1 at 87 bar	-	[23]
Cu-BTC	1507	2.50	-	-	[42]
Cu-BTC	1482	2.90	-	-	[43]
Cu-BTC	1055	1.95	-	0.47 at 303 K and 35 bar	[1]
Cu-BTC	1387	-	-	0.70 at 298 K and 45 bar	Present work

2.2.1.2 Hydrogen adsorption isotherm

For practical and design application, it is required to describe the equilibrium uptake of gases at different pressures by physical models. An adsorption model isotherm is a relationship which relates the amount of gas uptake by the adsorbent to the pressure in the gas bulk phase. It is well known that equilibrium adsorption of gases can be described by several model isotherms such as Langmuir and Freundlich as given below:

Langmuir: $$q_e = q_m \frac{K_L P}{1 + K_L P} \quad (1)$$

Freundlich: $$q_e = K_f P^{1/n} \quad (2)$$

where the equations parameters are q_m (wt%), maximum adsorption of adsorbent monolayer; K_L (bar^{-1}), Langmuir constant; K_f (bar $^{-1/n}$), Freundlich constant and n (-), Freundlich exponent. Nonlinear fit of experimental hydrogen uptake data at adsorption temperature of 298 K with Langmuir and Freundlich models are shown in Fig. 6. The models parameters are listed in Table 5.

Table 5: Langmuir and Freundlich isotherm constants for hydrogen adsorption on Cu-BTC adsorbent synthesized at different temperatures

Sample no.	Langmuir		R^2	Freundlich		R^2
	q_{max}	K_L		K_f	n	
Cu-BTC 75/80	2.8905	0.0067	0.9992	0.0256	1.1648	0.9989
Cu-BTC 75/110	3.3878	0.0052	0.9942	0.0230	1.1399	0.9951
Cu-BTC 75/140	6.3249	0.0023	0.9983	0.0161	1.0502	0.9979

According to model parameters and coefficients obtained from nonlinear fit, the Langmuir constant, K_L, increased when reaction temperature was decreased. Since K_L is the ratio of adsorption constant to desorption constant, promotion of this constant at lower temperature elucidates the predominance of H_2 adsorption over desorption process. Such enhancement in the hydrogen adsorption can be attributed to the increase of micropore volume along with decrease of synthesis temperature, as prior mentioned. The parameter n in the Freundlich model represents affinity of the adsorbent surface towards gas molecules. As the results show when the reaction temperature was raised, the value of parameter n decreased. This implies that the surface became more favourable for hydrogen adsorption at lower reaction temperature. By comparing the data obtained at various solvent contents and reaction temperatures (Figs. 5 and 6), it could be inferred that the solvent content is more influential factor than reaction temperature on hydrogen uptake by the synthetized Cu-BTC adsorbents.

2.2.2. Adsorption thermodynamics

The strength of interaction between adsorbent surface and adsorbate molecules is characterized by measuring isosteric heat of adsorption (Q_{st}) that is defined by Clausius–Clapeyron equation [6] :

$$Q_{st} = RT^2 \left(\frac{\partial \ln P}{\partial T} \right)_{q_e} \quad (3)$$

Hydrogen uptake data obtained at different temperatures were used to calculate heat of adsorption by Eq. (3). Table 6 represents the values of model parameters obtained using curve fitting toolbox of MATLAB software (Version 7.14). Both model isotherms used in this study represent the same accuracies in terms of fitting determination coefficient (R^2). Fig. 7 is nice to show this compliance.

RSC Advances RSCPublishing

ARTICLE

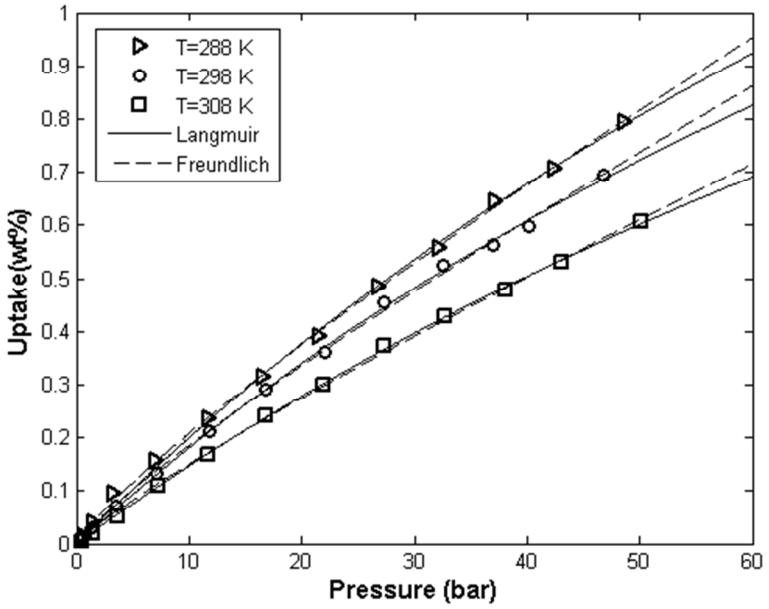

Fig.7. Hydrogen adsorption data and the fitted curves by Langmuir and Freundlich isotherms on the Cu-BTC 75/80 at 288, 298 and 308 K

Table 6: Langmuir and Freundlich isotherm constants for hydrogen adsorption on Cu-BTC 75/80 at 288, 298 and 308 K

Temperature	Langmuir		R^2	Freundlich		R^2
	q_{max}	K_L		K_f	n	
288 K	3.3590	0.0063	0.9983	0.0294	1.1773	0.9993
298 K	2.8905	0.0067	0.9992	0.0256	1.1648	0.9989
308 K	2.6785	0.0058	0.9996	0.0201	1.1468	0.9988

To calculate isosteric heat of adsorption, the Freundlich model (Eq. (2)) with following temperature dependent parameters was used [44]:

$$K_f = K_0 \exp(-\frac{\alpha RT}{A_0}) \quad , \quad \frac{1}{n} = \frac{RT}{A_0} \qquad (4)$$

where n is an assessment of interaction between adsorbate and adsorbent similar to isosteric heat of adsorption. Isosteric heat of adsorption was obtained by substitution of the Freundlich isotherm in the Clausius–Clapeyron equation according to Eq. (5):

$$Q_{st} = A_0 \ln(\frac{K_0}{q_e}) \qquad (5)$$

The coefficients and parameters of Eq. (5), which are presented in Table 7, were calculated based on all acquired experimental data at three different temperatures and in the pressure range of 0 to 45 bar following a multiple regression

procedure. Variation in heat of adsorption versus amount of uptake is shown in Fig.8. Initial Q_{st} of hydrogen for Cu-BTC at 0.05 wt% uptake is about 20.5 kJ/mol, which is more than the values reported for HKUST-1 (19.5 kJ/mol, as calculated by the authors of this work) [1] and UiO-66 (12 kJ/mol) [27] indicating a stronger interaction between hydrogen molecules and the adsorbent surface. The isosteric heat of adsorption decreased monotonically with increase of hydrogen surface loading due to weakening of interaction between hydrogen molecules and the adsorbent surface at high surface loadings.

Table 7: Isosteric heat of adsorption parameters obtained based on the Freundlich model isotherm with temperature dependent parameters for adsorption of hydrogen on Cu-BTC 75/80

Parameters	A_0	A	K_0
Value	2613.64	9.33	130.58

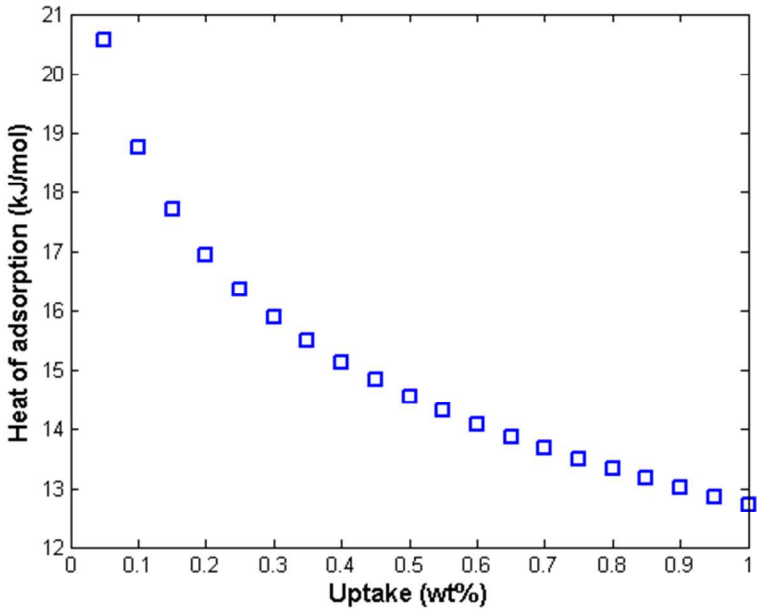

Fig.8. Isosteric heat of hydrogen adsorption on Cu-BTC 75/80 as a function of uptake predicted from the Freundlich model isotherm with temperature dependent parameters

2.2.3. H_2 adsorption kinetics

Study of the mechanism of an adsorption system including physisorption and chemisorption is frequently carried out by reaction models such as pseudo-first-order and pseudo-second-order kinetic models. In this study, an arbitrary *n*-th order model was used in which the order of adsorption reaction was considered as an adjustable parameter. The pseudo-*n*-th-order kinetic equation is presented as follows:

$$\frac{dq}{dt} = K_n (q_e - q)^n \quad (6)$$

where q_e is the capacity of adsorption at equilibrium state, K_n is the rate constant and n is the order of kinetic model. Eq. (7) is obtained by integration of Eq. (6):

$$q_t = q_e - [(q_e)^{1-n} + (n-1)K_n t]^{\frac{1}{1-n}} \quad (7)$$

The parameters n, K_n and q_e were obtained by fitting kinetics data with Eq. (7). The task was performed by considering the curve fitting problem as an optimization issue. This problem was solved by a genetic algorithm code that had been written to fit data. Objective function for the convergence of optimization program was defined by Eq. (8):

$$Error = \frac{1}{N}\sum_{i=1}^{N}\left(q_{model}(T,P) - q_{\exp}(T,P)\right)^2 \quad (8)$$

Fig. 9 reveals the results of applying n-th order kinetic model to describe hydrogen adsorption kinetic data on Cu-BTC MOF synthesized at 80 °C, at 298 K and 20 bar. The kinetic model parameters obtained through nonlinear fit of experimental data are listed in Table 8. The value of adjustable parameter n which represents the order of adsorption reaction was obtained as 1.59, which lies between 1 and 2 indicating that the adsorption process was controlled by a combination of physisorption and chemisorption mechanisms. The pseudo-first-order reaction is obtained by putting n=1 in Eq. (6). The fitting results based on this kinetic model are also presented in Fig. 9 for comparison. The figure obviously shows the superior prediction performance of the n-th order kinetic model compared to the first-order model.

Table 8: Pseudo-first and n-th order kinetic models constants for hydrogen adsorption on Cu-BTC 75/80 at 298 K and 20 bar.

$q_{e(exp)}$	n-th order				First-order		
	q_e	n	K_n	R^2	q_e	K_1	R^2
0.324	0.325	1.59	0.842	0.9986	0.299	0.382	0.9868

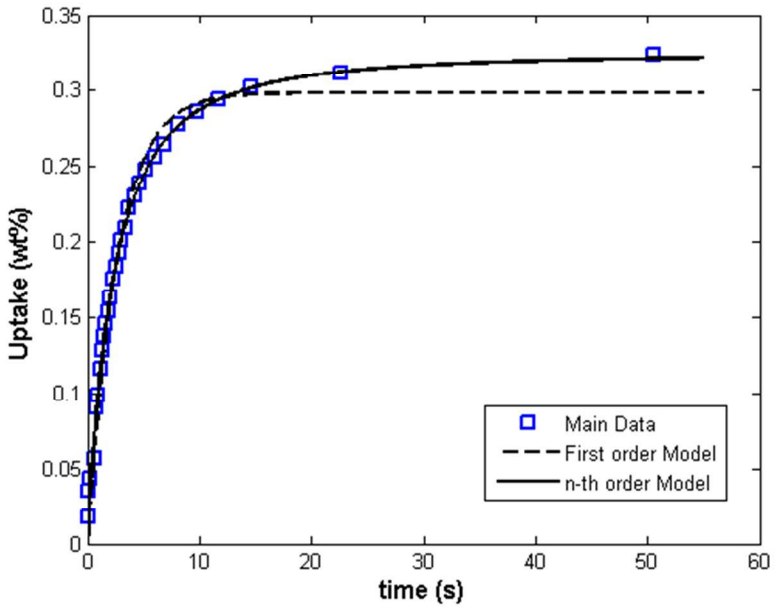

Fig.9. Kinetic data of H_2 adsorption on Cu-BTC 75/80 and the fitted curves with pseudo n-th order and pseudo first order kinetic model at 298 K and 20 bar

Conclusion

This study demonstrated that Cu-BTC MOF synthesized at atmospheric pressure using ultrasonic followed by reflux method

could adsorb large amount of hydrogen. Increasing the synthesis temperature reduced the crystallinity of the developed MOFs and led to a decrease in total pore volume, micropore volume and BET surface area of the samples. It was found that increasing solvent content during synthesis of Cu-BTC was effective in enhancement of hydrogen uptake to a certain extent. The equilibrium uptake of hydrogen was equally well fitted by the Freundlich and Langmuir model isotherms. Heat of adsorption was calculated by applying Freundlich isotherm with temperature dependent parameters in Clausius–Clapeyron equation. Maximum heat of adsorption was computed to be 20.5 kJ /mol at 0.05 wt% uptake from the corresponding isotherms at 288, 298 and 308 K. Also, an *n*-th order kinetic model was used to describe the experimental kinetic data. The three parameters *n*-th order kinetic model could give a better description for the kinetic data compared to the conventional pseudo-first-order model. The value of 1.59 obtained for the order of kinetic model indicated that the adsorption process was controlled by a combination of physisorption and chemisorption.

Notes and references

[a] Chemical Engineering Department, Babol University of Technology, Shariati Street, Babol 4714871167, Iran.
* Corresponding author. Tel. /Fax: +98 11 23234204.
E-mail addresses: aa_ghoreyshi@nit.ac.ir, aa_ghoreyshi@yahoo.com (A.A.Ghoreyshi).

1. K.-S. Lin, A. K. Adhikari, C.-N. Ku, C.-L. Chiang and H. Kuo, *International Journal of Hydrogen Energy*, 2012, **37**, 13865-13871.
2. Q. Zheng, X. Wang and S. Gao, *Cryogenics*, 2014, **61**, 143-148.
3. M. Fujiwara, Y. Fujio, H. Sakurai, H. Senoh and T. Kiyobayashi, *Chemical Engineering and Processing: Process Intensification*, 2014, **79**, 1-6.
4. M. Delavar, A. Asghar Ghoreyshi, M. Jahanshahi, S. Khalili and N. Nabian, *RSC Advances*, 2012, **2**, 4490-4497.
5. S. Khalili, A. A. Ghoreyshi, M. Jahanshahi and K. Pirzadeh, *CLEAN – Soil, Air, Water*, 2013, **41**, 939-948.
6. M. Keramati and A. A. Ghoreyshi, *Physica E: Low-dimensional Systems and Nanostructures*, 2014, **57**, 161-168.
7. K. V. Kumar, M. C. M. d. Castro, M. Martinez-Escandell, M. Molina-Sabio and F. Rodriguez-Reinoso, *Chemical Engineering Journal*, 2011, **168**, 972-978.
8. N. L. Rosi, J. Eckert, M. Eddaoudi, D. T. Vodak, J. Kim, M. O'Keeffe and O. M. Yaghi, *Science*, 2003, **300**, 1127-1129.
9. A. Banerjee, U. Singh, V. Aravindan, M. Srinivasan and S. Ogale, *Nano Energy*, 2013, **2**, 1158-1163.
10. A. Bertucci, A. Manicardi, A. Candiani, S. Giannetti, A. Cucinotta, G. Spoto, M. Konstantaki, S. Pissadakis, S. Selleri and R. Corradini, *Biosensors and Bioelectronics*, 2015, **63**, 248-254.
11. A. Shahat, H. M. A. Hassan and H. M. E. Azzazy, *Analytica Chimica Acta*, 2013, **793**, 90-98.
12. N. Motakef-Kazemi, S. A. Shojaosadati and A. Morsali, *Microporous and Mesoporous Materials*, 2014, **186**, 73-79.
13. K. Schlichte, T. Kratzke and S. Kaskel, *Microporous and Mesoporous Materials*, 2004, **73**, 81-88.
14. L. T. L. Nguyen, T. T. Nguyen, K. D. Nguyen and N. T. S. Phan, *Applied Catalysis A: General*, 2012, **425–426**, 44-52.
15. M. Anbia and V. Hoseini, *Chemical Engineering Journal*, 2012, **191**, 326-330.
16. M. Anbia and S. Sheykhi, *Journal of Industrial and Engineering Chemistry*, 2013, **19**, 1583-1586.
17. Z.-Q. Li, L.-G. Qiu, T. Xu, Y. Wu, W. Wang, Z.-Y. Wu and X. Jiang, *Materials Letters*, 2009, **63**, 78-80.
18. Z. Xiang, Z. Hu, W. Yang and D. Cao, *International Journal of Hydrogen Energy*, 2012, **37**, 946-950.
19. X. Yan, S. Komarneni, Z. Zhang and Z. Yan, *Microporous and Mesoporous Materials*, 2014, **183**, 69-73.
20. Q. Min Wang, D. Shen, M. Bülow, M. Ling Lau, S. Deng, F. R. Fitch, N. O. Lemcoff and J. Semanscin, *Microporous and Mesoporous Materials*, 2002, **55**, 217-230.
21. H. Furukawa, N. Ko, Y. B. Go, N. Aratani, S. B. Choi, E. Choi, A. Ö. Yazaydin, R. Q. Snurr, M. O'Keeffe, J. Kim and O. M. Yaghi, *Science*, 2010, **329**, 424-428.
22. L. J. Murray, M. Dinca and J. R. Long, *Chemical Society Reviews*, 2009, **38**, 1294-1314.
23. A. G. Wong-Foy, A. J. Matzger and O. M. Yaghi, *Journal of the American Chemical Society*, 2006, **128**, 3494-3495.
24. H. K. Chae, D. Y. Siberio-Perez, J. Kim, Y. Go, M. Eddaoudi, A. J. Matzger, M. O'Keeffe and O. M. Yaghi, *Nature*, 2004, **427**, 523-527.
25. Y. Li and R. T. Yang, *Langmuir*, 2007, **23**, 12937-12944.
26. D. Saha, Z. Wei and S. Deng, *International Journal of Hydrogen Energy*, 2088, **33**, 7479-7488.
27. H. R. Abid, H. Tian, H.-M. Ang, M. O. Tade, C. E. Buckley and S. Wang, *Chemical Engineering Journal*, 2012, **187**, 415-420.
28. S. S. Y. Chui, S. M. F. Lo, J. P. H. Charmant, A. G. Orpen and I. D. Williams, *Science*, 1999, **283**, 1148-1150.
29. R. Sabouni, H. Kazemian and S. Rohani, *Microporous and Mesoporous Materials*, 2013, **175**, 85-91.
30. M. A. Alavi, A. Morsali, S. W. Joo and B.-K. Min, *Ultrasonics Sonochemistry*, 2015, **22**, 349-358.
31. H. Yang, S. Orefuwa and A. Goudy, *Microporous and Mesoporous Materials*, 2011, **143**, 37-45.

32. C.-P. Li and M. Du, *Chemical Communications*, 2011, **47**, 5958-5972.
33. L.-S. Long, *CrystEngComm*, 2010, **12**, 1354-1365.
34. L. Luo, G.-C. Lv, P. Wang, Q. Liu, K. Chen and W.-Y. Sun, *CrystEngComm*, 2013, **15**, 9537-9543.
35. B. Xiao and Q. Yuan, *Particuology*, 2009, **7**, 129-140.
36. M. Chen, M.-S. Chen, T.-a. Okamura, M.-F. Lv, W.-Y. Sun and N. Ueyama, *CrystEngComm*, 2011, **13**, 3801-3810.
37. P. Mahata, A. Sundaresan and S. Natarajan, *Chemical Communications*, 2007, 4471-4473.
38. E.-C. Yang, T.-Y. Liu, Q. Wang and X.-J. Zhao, *Inorganic Chemistry Communications*, 2011, **14**, 285-287.
39. L.-F. Ma, L.-Y. Wang, D.-H. Lu, S. R. Batten and J.-G. Wang, *Crystal Growth & Design*, 2009, **9**, 1741-1749.
40. P. M. Forster, A. R. Burbank, C. Livage, G. Ferey and A. K. Cheetham, *Chemical Communications*, 2004, 368-369.
41. S. R. Venna, J. B. Jasinski and M. A. Carreon, *Journal of the American Chemical Society*, 2010, **132**, 18030-18033.
42. J. L. C. Rowsell and O. M. Yaghi, *Journal of the American Chemical Society*, 2006, **128**, 1304-1315.
43. J. Liu, J. T. Culp, S. Natesakhawat, B. C. Bockrath, B. Zande, S. G. Sankar, G. Garberoglio and J. K. Johnson, *The Journal of Physical Chemistry C*, 2007, **111**, 9305-9313.
44. D. D. Do, *Adsorption analysis : equilibria and kinetics*, Imperial College Press, London, 1998.

